Remote Sensing of Environment 115 (2011) 3640–3646

Contents lists available at SciVerse ScienceDirect

Remote Sensing of Environment

journal homepage: www.elsevier.com/locate/rse

# Broadband, red-edge information from satellites improves early stress detection in a New Mexico conifer woodland

Jan U.H. Eitel [a,b,*], Lee A. Vierling [a], Marcy E. Litvak [c], Dan S. Long [d], Urs Schulthess [e], Alan A. Ager [f], Dan J. Krofcheck [c], Leo Stoscheck [c]

[a] Geospatial Laboratory for Environmental Dynamics, University of Idaho, Moscow, ID 83844-1135, USA
[b] McCall Outdoor Science School, University of Idaho, McCall, ID 83638, USA
[c] University of New Mexico, Biology Department, Albuquerque, NM 87131-0001, USA
[d] Columbia Plateau Conservation Research Center, PO Box 370, Pendleton, OR 97801, USA
[e] RapidEye AG, Molkenmarkt 30, 14776 Brandenburg an der Havel, Germany
[f] Western Wildlands Environmental Threat Assessment Center, USDA Forest Service, Pacific Northwest Research Station, Prineville, OR 97754, USA

ARTICLE INFO

*Article history:*
Received 26 May 2011
Received in revised form 31 August 2011
Accepted 3 September 2011
Available online 19 October 2011

*Keywords:*
Chlorophyll a/b ratio
Forest health
Piñon-juniper woodland
*Pinus edulis*
*Juniperus monosperma*
Stress detection

ABSTRACT

Multiple plant stresses can affect the health, esthetic condition, and timber harvest value of conifer forests. To monitor spatial and temporal dynamic forest stress conditions, timely, accurate, and cost-effective information is needed that could be provided by remote sensing. Recently, satellite imagery has become available via the RapidEye satellite constellation to provide spectral information in five broad bands, including the red-edge region (690–730 nm) of the electromagnetic spectrum. We tested the hypothesis that broadband, red-edge satellite information improves early detection of stress (as manifest by shifts in foliar chlorophyll a + b) in a woodland ecosystem relative to other more commonly utilized band combinations of red, green, blue, and near infrared band reflectance spectra. We analyzed a temporally dense time series of 22 RapidEye scenes of a piñon-juniper woodland in central New Mexico acquired before and after stress was induced by girdling. We found that the Normalized Difference Red-Edge index (NDRE) allowed stress to be detected 13 days after girdling — between and 16 days earlier than broadband spectral indices such as the Normalized Difference Vegetation Index (NDVI) and Green NDVI traditionally used for satellite based forest health monitoring. We conclude that red-edge information has the potential to considerably improve forest stress monitoring from satellites and warrants further investigation in other forested ecosystems.



## 1. Introduction

Stressors affecting forests are highly dynamic in space and time and therefore can affect the health, esthetic condition, and ecosystem services provided by forests in multiple ways. Due to tight coupling among temperature, precipitation, and various types of plant stressors, climate change might intensify the effects of stress on forests (Logan et al., 2003; Niinemets, 2010). For instance, predicted warming surface temperatures and droughts in North American forests are expected to result in more intensified insect outbreaks (Logan et al., 2003). This development is of great socio-economic importance given that forest insects and disease are already the main agents of natural disturbance in North American forests. Remarkably, relative to fire, insects and pathogens impact 45 times more forest area in the US and have a fivefold greater economic impact (Logan et al., 2003). Timely, accurate, and cost-effective information is therefore needed via remote sensing to monitor spatio-temporal dynamics of forest stress conditions, test ecological hypotheses related to forest stress, and guide the allocation of resources for stress mitigation and control (e.g., sanitation logging) (Pontius et al., 2005; Wulder et al., 2005). Further, maps of remotely sensed stress and mortality at multiple scales could provide insight into the dynamics of stress and mortality patterns caused by different agents of stress in a changing climate (Hatala et al., 2010).

Plants experience stress if suboptimal growth conditions cause their plant physiological functions (e.g., light and dark reactions of photosynthesis) to decline from their physiological standard (Niinemets, 2010). To be of value for forest health monitoring, stress detection should be early to allow timely intervention and minimize the spread of stress agents. Numerous studies have explored the utility of remote sensing for early stress detection. Spectral vegetation indices (SVIs) have been investigated that employ short-wave infrared wavelengths sensitive to plant water content (e.g. Ceccato et al., 2001; Eitel et al.,

* Corresponding author at: Geospatial Laboratory for Environmental Dynamics, University of Idaho, Moscow, ID 83844-1135, USA. Tel.: +1 208 596 9277.
*E-mail addresses:* jeitel@vandals.uidaho.edu (J.U.H. Eitel), leev@uidaho.edu (L.A. Vierling), mlitvak@unm.edu (M.E. Litvak), dan.long@ars.usda.gov (D.S. Long), schulthess@rapideye.de (U. Schulthess), aager@fs.fed.us (A.A. Ager), krofcheck@gmail.com (D.J. Krofcheck).

0034-4257/$ – see front matter © 2011 Elsevier Inc. All rights reserved.
doi:10.1016/j.rse.2011.09.002

2006; Stimson et al., 2005; Toomey & Vierling, 2005). The use of SVIs using visible bands such as the Normalized Difference Vegetation Index (NDVI; Tucker, 1979) can also be useful because a wide variety of different stress agents such as temperature, light, disease, ozone, or plant nutrition induce the loss of chlorophyll a + b ($Chl_{ab}$) which strongly affects absorption of photosynthetically active radiation (Carter, 1993; Carter & Knapp, 2001; Hendry et al., 1987). As a result, increasing visible reflectance has shown to be one of the most universal responses of leaf spectral reflectance to stress (Carter, 1993; Carter & Knapp, 2001). Within the visible spectrum, reflectance bands centered within the red (670 nm) and the green (550 nm) spectral regions have generally been used to remotely detect stress from satellite platforms. However, $Chl_{ab}$ strongly absorbs in the red spectral region, leading to red reflectance saturation at low $Chl_{ab}$ levels and making the red band often unresponsive to an initial loss in $Chl_{ab}$ at earlier stress stages (Carter & Knapp, 2001; Jacquemoud & Baret, 1990). This explains the finding by Carter (1993) who showed a sensitivity minimum in the red (centered at 670 nm) to eight different stress agents (competition, herbicide, pathogen, ozone, insufficient mycorrhizae, barrier island environment, senescence, and dehydration). In contrast to red reflectance, green (centered at 550 nm) and red-edge (centered at 700 nm) reflectances have been found to be sensitive to a wide range of $Chl_{ab}$ levels. Between the green and the red-edge reflectances there is evidence that the wavelength in the red-edge region is superior to the green in regards to its responsiveness to stress induced changes in $Chl_{ab}$ (Carter, 1993, 1998; Carter & Knapp, 2001; Carter & Miller, 1994; Eitel et al., 2007, 2008, 2009, 2010). This might be partly due to the red-edge band picking up some stress induced increase in fluorescence (Carter & Miller, 1994; Lichtenthaler & Rinderle, 1988).

Findings by Carter and Miller (1994) indicated that the ratio of red-edge (690–700) to NIR (760 nm) reflectance could improve early stress detection in soybean. This ratio corresponded more closely to plant physiological measures of stress (fluorescence and plant water status) than wavebands and waveband combinations in the visible-NIR region of the electromagnetic spectrum. Carter and Knapp (2001) studied the effect of a wide variety of stressors (dehydration, flooding, freezing, ozone, herbicides, competition, diseases, insects, N fertilization) on the spectral response between 400 and 850 nm of different plant species including conifers and deciduous trees. They found that, within that range of wavelengths, an increase in reflectance at 700 nm was the most universal and most sensitive spectral response of plants to stress. In Balsam fir (*Abies balsamea* (L.) Mill), Luther and Carroll (1999) showed that the red-edge reflectance at 711 nm was most sensitive to stress induced by root pruning, light, and nutrient availability. Eitel et al. (2010) showed for Scots pine (*Pinus sylvestris*) that red-edge reflectance information improved active ground optical remote sensing estimates of stress induced changes in $Chl_{ab}$ ($r^2 > 0.73$) over those based on red wavelength (590–670 nm) information ($r^2 = 0.57$). Narrow band reflectance imagery acquired from a ground-based platform that provided red-edge reflectance information (695 ± 5 nm) allowed detecting herbicide-induced stress in loblolly pine (*Pinus taeda L.*) and slash pine (*Pinus elliottii Engelm.*) 16 days prior to visual signs of stress (Cater et al., 1996).

These findings suggest that the use of red-edge information could help to improve the early detection of plant stress. However, most of the aforementioned studies were not based on satellite data. An explanation for the latter is that until recently, only a limited number of hyperspectral satellite platforms provided radiance data in the red-edge portion of the spectrum, while multispectral satellites such as Landsat did not provide red-edge information. This recently changed with the launches of the RapidEye (Brandenburg, Germany) and DigitalGlobe WorldView-2 (Longmont, CO, USA) satellites now providing commercially available red-edge band information. As many of the studies employing red-edge information were based on narrow band (=<10 nm FWHM spectral sampling) ground spectral data, relatively little is known if broadband, red-edge satellite data (>10 nm) can respond to and assist with tracking stress induced changes that have been reported for narrow band red-edge reflectance.

The objective of this study was to determine whether broadband, red-edge information from the RapidEye satellites improves early stress detection in conifer forests relative to information provided by combinations of other non red-edge spectral bands. We addressed this objective by examining the utility of red-edge and non red-edge indices for early stress detection. Spectra used for this analysis were simulated with the PROSPECT + SAIL radiative transfer model and acquired with the RapidEye satellite constellation. The use of a physically based canopy reflectance model allowed us to simulate satellite spectra for varying levels of $Chl_{ab}$ while holding other variables (e.g., leaf area index (LAI), viewing and illumination geometry) constant that may complicate the interpretation of these data when actual satellite data are used. By evaluating the simulated satellite spectra combined with a temporally dense time series of satellite data for $Chl_{ab}$-related stress detection, we aim to shed light on improving satellite-based early warning systems and to guide future earth observing satellite designs for future monitoring of forest stress.

## 2. Methods

### 2.1. PROSPECT + SAIL simulations

The PROSPECT radiative transfer model (Jacquemoud & Baret, 1990) was used to simulate leaf reflectance and transmittance spectra between 400 and 900 nm at a spectral resolution of 1 nm. Model input parameters are leaf structural parameter N, leaf water content Cw, leaf dry matter content Cdm (g $cm^{-2}$), and leaf $Chl_{ab}$ (μg $cm^{-2}$). Thirteen simulated leaf reflectance and transmittance spectra were obtained with typical evergreen needle values (Ollinger, 2011) for N = 1.0, Cw = 0.02 cm and Cdm = 0.02 g $cm^{-2}$, and $Chl_{ab}$ ranging between 0 and 65 μg $cm^{-2}$ (approximate $Chl_{ab}$ range observed in a pinion-juniper woodland by Eitel et al., 2011) in 5 μg $cm^{-2}$ increments. Canopy reflectance was simulated using the SAIL canopy model (Verhoef, 1984) for MS-Windows (WinSAIL v.1.00.04., USDA-ARS Hydrology and Remote Sensing Laboratory, Beltsville, MD, USA). Model inputs consisted of the following viewing/illumination parameters that were kept constant between model runs: latitude, solar declination angle, constant leaf angle distribution of 20° (Ollinger, 2011), sensor viewing angle, sensor zenith angle, time of day, fraction of direct solar irradiance, and soil background reflectance. Soil reflectance was the mean of four representative soil spectra collected at the study site (described under Section 2.2.1 below) with a ASD FieldSpec® HandHeld spectroradiometer (Analytical Spectral Devices, Boulder, Colorado, USA). SAIL was then run with a LAI value of 1.13 for each of the 14 leaf reflectance and transmittance spectra that had been simulated with PROSPECT for the different $Chl_{ab}$ values. The average LAI value was determined based on 60 LAI measurements that were taken with a LI-COR model LAI-2000 plant canopy analyzer (LI-COR, Lincoln, NE) at the study site at the beginning of the study. The hyperspectral reflectance data simulated by PROSPECT + SAIL were converted to band equivalent reflectance (BER) of the RapidEye satellites using the following equation (Trigg & Flasse, 2000):

$$R_x = \frac{\sum_{i=\lambda_{min}}^{\lambda_{max}} r_i \rho_i}{\sum_{i=\lambda_{min}}^{\lambda_{max}} r_i} \quad (1)$$

where $R_x$ = the BER for band $x$; $\lambda_{min}$ = starting wavelength of band $x$'s filter function; $\lambda_{max}$ = ending wavelength of band $x$'s filter function; $r_i$ = relative response in reflectance for band $x$ at wavelength $i$; and $\rho_i$ = reflectance simulated at wavelength $i$.

Three different spectral vegetation indices (SVI) were extracted from the simulated spectra: the Normalized Difference Vegetation Index (NDVI), the Green Normalized Vegetation Index (GNDVI), and the Normalized Red Edge Index (NDRE) (Table 1). These indices were selected because they all employ a NIR band but differ in terms of the second, $Chl_{ab}$ sensitive band they employ. Specifically, NDVI employs the red band, GNDVI the green band, and NDRE the red-edge band.

### 2.2. Satellite and field observations

#### 2.2.1. Study site

At an eddy covariance flux tower site, 4 ha control site (hereafter referred to as control-1-site) and 4 ha treatment site were established in a semiarid piñon-juniper woodland just South of Mountainair, NM (34.44649° N, 106.21446° W). A second 4 ha control site (hereafter referred to as control-2-site) was established at another nearby (<5 km, 34.438450° N, −106.237694° W) eddy covariance flux tower site that experienced similar growth conditions throughout the experiment as the control-1-site. A second control site was needed to detrend the control-1-site data as outlined below under Section 2.2.3. The dominant tree species at the sites are *Pinus edulis* and *Juniperus monosperma*. The dominant herbaceous plant at the sites is the C4 perennial grass *Bouteloua gracilis*. On September 10th, 2009, ~1600 piñon trees (all >7 cm diameter at breast height) in the treatment site were girdled using chainsaws to sever the phloem at breast height. Fifty percent glyphosate was also injected into the girdled wound of each tree at this time to hasten the treatment effect.

#### 2.2.2. Plant material and analysis

Measures of the foliar chlorophyll a/b ratio were taken at the treatment and control-1-site as a plant physiological measure of girdling induced stress. The chlorophyll a/b ratio instead of $Chl_{ab}$ was used in this study as a physiological measure of plant stress since it has been identified as a sensitive indicator of girdling induced stress (Alonso et al., 2002).

Needle-leaf samples of piñon trees were collected shortly before girdling and eight times thereafter to approximately coincide with the satellite image acquisitions described below in Section 2.2.3. At both sites, needles from 36 piñon trees were randomly sampled at approximately the same crown position (upper crown). Immediately after sampling, each sample was placed in a sealable aluminum foil packet. Samples were packed in dry ice for their preservation during shipping to the laboratory. In the laboratory, a tissue sample of approximately 0.1 g was randomly taken from each leaf sample and cut into fine pieces (<0.25 $mm^2$). $Chl_{ab}$ was extracted from the leaf tissue using 80% acetone as the extraction solvent (MacKinney, 1941). Solutions were stored for up to 48 h in darkness (to prevent $Chl_{ab}$ degradation) until all $Chl_{ab}$ was extracted as indicated by white visual appearance of the leaf tissue. $Chl_{ab}$ extracts were then filtered and the absorbancy was measured at 644 nm and 663 nm with a Thermo scientific GENESYS 20™ visible spectrophotometer (Thermo Fisher Scientific Inc., MA, USA). The $Chl_a$ and $Chl_b$ of the chlorophyll extract solution were calculated with coefficients determined by Lichtenthaler and Wellburn (1983) in units of $\mu g\ g^{-1}$.

**Table 1**
Spectral indices calculated in this study. Band numbers refer to RapidEye band 2 (520–590 nm), band 3 (630–685 nm), band 4 (690–730 nm), and band 5 (760–850 nm).

| Vegetation index | Equation | Reference |
|---|---|---|
| Normalized difference Vegetation index (NDVI) | $NDVI = (R_{band5} - R_{band3})/(R_{band5} + R_{band3})$ | Tucker (1979) |
| Green normalized difference Vegetation index (GNDVI) | $GNDVI = (R_{band5} - R_{band2})/(R_{band5} + R_{band2})$ | Gitelson et al. (1996) |
| Normalized difference Red-Edge index (NDRE) | $NDRE = (R_{band5} - R_{band4})/(R_{band5} + R_{band4})$ | Barnes et al. (2000) |

The onset of stress in this study was defined by a statistically significant drop of the chlorophyll a/b ratio when compared to the chlorophyll a/b ratio before the girdling event. A probability level of $P<0.05$ was considered to be statistically significant. All statistical analysis for this study was conducted in the open-source statistical software package R 2.12.0 (R Core Team, 2010).

#### 2.2.3. Satellite image acquisition, pre-processing, and analysis

A total of 22 RapidEye satellite images of the study site were acquired between 7-Sept. 2009 and 21-Aug. 2010. Five images acquired between December 2009 and April 2010 were removed from the dataset due to snow in the imaged scene that confounded the spectral signal. Level 3A RapidEye images were used as an input with a pixel size of 5.0 m. The images were radiometrically and geometrically corrected (RapidEye AG, 2011). A noise filter and top of atmosphere (TOA) dark object subtraction were applied to each image. Residual geometric error was corrected by manually georegistering all images to a reference image using 10 ground control points and a polynomial warping method (ENVI 4.5, ITT Visual Information Solutions, Boulder, CO). The resulting root mean square error (RMSE) of position for each geometric correction was kept below one pixel (0.4 pixels or 2 m).

Girdled trees in the treatment site and non-girdled trees in the control sites were visually identified on a 19-Aug. 2010 false-color image (NIR band assigned to red color gun, red-edge band assigned to green color gun, and red band assigned to blue color gun). In this image collected 343 days post-girdling, girdled trees appeared brown whereas non-girdled trees appeared green. A total of 120 pixels were analyzed: 40 pixels were identified by a trained interpreter as girdled trees at the treatment site, and two additional sets of 40 pixels each were identified by the interpreter as non-girdled trees within both of the control sites.

After calculating the NDVI, GNDVI, and NDRE values from the satellite imagery, SVIs were detrended to remove trends extraneous to the girdling event (e.g. caused by BRDF effects, phenological changes to weather events) that confounded the stress signal. The detrending algorithm employed was based on the rationale that variability of spectral indices at an unstressed control site can be assumed to be caused by extraneous trends and not plant stress. Consequently, variability of undetrended spectral indices that corresponded with the variability of spectral indices at unstressed control sites (i.e. control-1-site and control-2-site) was not caused by the girdling event and was thus removed to isolate a potential stress signal.

For the detrending, a linear regression model was fit between the SVIs extracted from the treatment (y) and the control-1-site (x) to determine the variability of spectral indices (dependent variable) at the treatment site that corresponded with variability of spectral indices (independent variable) at control-1 site:

$$y = \alpha + \beta x + \varepsilon. \quad (2)$$

The intercept ($\alpha$) and slope ($\beta$) of the linear regression model capturing the trend between the two sites were then used to detrend the pixel values and thus isolate a potential stress signal by subtracting the trend as follows:

$$yd = y - (\alpha + \beta x_i) \quad (3)$$

where yd are the detrended spectral index (SI) values, y are the undetrended SI values, and x are the SI values associated with the independent variable used to fit the linear regression model in Eq. (2). Following the procedure above, the index values of the control-1-site were also detrended. To detrend the control-1-site, a second control site (control-2-site) was identified for which spectral index values were unaffected by plant stress and thus could be used as the independent variable in Eqs. (2) and (3). The spectral index values of the treatment site could not be used to detrend the control-1-site data because

using them as the independent variable in Eqs. (2) and (3) would violate the basic assumption of the detrending algorithm that assumes that the variability of spectral index values used as independent variable in Eqs. (2) and (3) are caused only by extraneous factors and not plant stress.

For each SVI, a "no change" region was defined by using the 25th and 75th percentile of SVI values measured within the treatment and control areas prior to girdling (07–09 Sept. 2009). An area was classified as stressed if the 75th percentile of SVI values within the studied area dropped below the "no change" region.

## 3. Results and discussion

The PROSPECT + SAIL model allowed us to simulate satellite spectra by varying $Chl_{ab}$ while holding constant other variables such as LAI, leaf angle distribution, and viewing and illumination geometry. This modeling approach is a useful diagnostic technique that can be used to complement real satellite data, where it is more difficult to separate and thus interpret the effects of the variable of interest from the effects of other variables. The PROSPECT + SAIL simulation results thus helped in interpreting the satellite data based results of this study. Though the PROSPECT + SAIL model did not allow for simulation of the effect of changes in chlorophyll a/b ratio on leaf reflectance and transmittance spectra per se, it integrated the effect of variations in $Chl_a$ and $Chl_b$ concentration on leaf reflectance and transmittance spectra and thus should allow to obtain a reasonable understanding about the responsiveness of spectral indices to both changes in $Chl_{ab}$ and the chlorophyll a/b ratio.

The PROSPECT + SAIL simulation showed that NDVI saturates at $Chl_{ab} > 30\ \mu g\ cm^{-2}$ (Fig. 1). In contrast, both GNDVI and NDRE remained sensitive over the entire range in $Chl_{ab}$ from 0 to $65\ \mu g\ cm^{-2}$. The saturation of NDVI at low $Chl_{ab}$ levels can be attributed to NDVI employing red reflectance in contrast to GNDVI employing green reflectance and NDRE employing red-edge reflectance. This finding illustrates the inherent limitation of NDVI for stress detection in forests. Strong $Chl_{ab}$ absorption in the red causes saturation of red reflectance at low $Chl_{ab}$ concentrations. Consequently, NDVI is insensitive to changes in $Chl_{ab}$ for moderate to high concentrations of leaf $Chl_{ab}$. Green and red-edge bands are less affected by $Chl_{ab}$ absorption, but do not saturate at medium to high $Chl_{ab}$ concentrations. Arguably, this limitation might be less of an issue when NDVI is employed for remote stress detection in conifers characterized by lower $Chl_{ab}$ levels, but should become more of an issue if NDVI is used to detect stress in broadleaves, which are generally characterized by higher $Chl_{ab}$ levels (Eitel et al., 2011; Ollinger, 2011).

The laboratory-measured chlorophyll a/b ratio of the control-1-site increased with time between one and 19 days since girdling, followed by a decrease in the chlorophyll a/b ratio (Fig. 2). The chlorophyll a/b ratio might have been increased by enhanced moisture availability and improved growth conditions resulting from rainfall events during August and September that caused higher moisture availability and thus improved growth conditions. Though no chlorophyll a/b ratio was measured at the control-2-site, no visual changes in greenness were observed at the control-2-site throughout the experiment. The chlorophyll a/b ratio in the treatment site significantly decreased ($p<0.05$) between 12 and 19 days since girdling. Another pronounced drop in the chlorophyll a/b ratio occurred between 240 and 309 days post girdling. The chlorophyll a/b ratio varied widely during the 213 days post girdling (both treatment and control-1-site) and 309 days since girdling (only in the control-1-site). The reasons for this are unknown.

A change in foliage color from dark to light green became visually apparent 10 days after girdling (sensu Fig. 3). Changes in greenness became first visibly apparent at the top of the canopy. Though we did not specifically measure leaf area after the girdling event, significant needle drop and changes in leaf area were not observed until 300 days after girdling.

Spectral indices in the control and treatment sites co-varied throughout the experiment likely due to BRDF and/or some atmospheric effects that were not accounted for in the preprocessing steps (Fig. 4). We removed these underlying trends by detrending these data as described in the Methods section. After detrending, all SVIs extracted from the control-1-site remained within the no change region (Fig. 4c, g, k). In contrast, SVIs of the treatment site each dropped below the "no change" region after the girdling event (Fig. 4d, h, l). However, the point in time during which SVIs dropped below the "no change" region differed among spectral indices. NDRE-based analyses revealed a drop below the "no change" region 13 days after girdling (Fig. 4l), which approximately coincided with the significant drop in the laboratory-measured chlorophyll a/b ratio between 12 and 19 days after girdling. Both GNDVI and NDVI dropped below the "no change" 16 days later (Fig. 4d, h).

These results broadly agree with ground-based results of Carter (1998) and Carter et al. (1996). Carter (1998) showed that stress induced changes in photosynthetic capacity of loblolly pine and slash pine correlated most strongly with NDRE ($r^2 = 0.75$) followed by NDVI ($r^2 = 0.54$), and GNDVI ($r^2 = 0.46$). In another study, Carter et al. (1996) showed that the narrow band reflectance ratio between the red-edge (694 nm) and near infrared (760 nm) reflectance was most effective for early stress detection in loblolly pine and slash pine within the 350 to 850 nm range. They showed that the 694/760 nm reflectance ratio allowed plant stress to be detected 16 days before signs of stress became visually apparent. Our results agree with previous studies that found red-edge band information

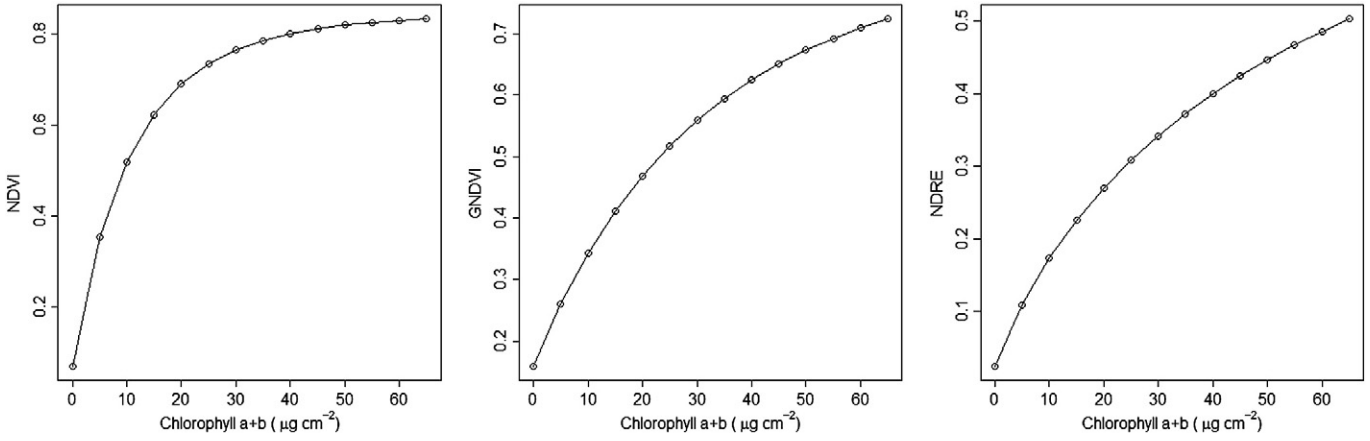


**Fig. 1.** Modeled spectral indices as a function chlorophyll a + b ($Chl_{ab}$) content ranging between 0 and $65\ \mu g\ cm^{-2}$.

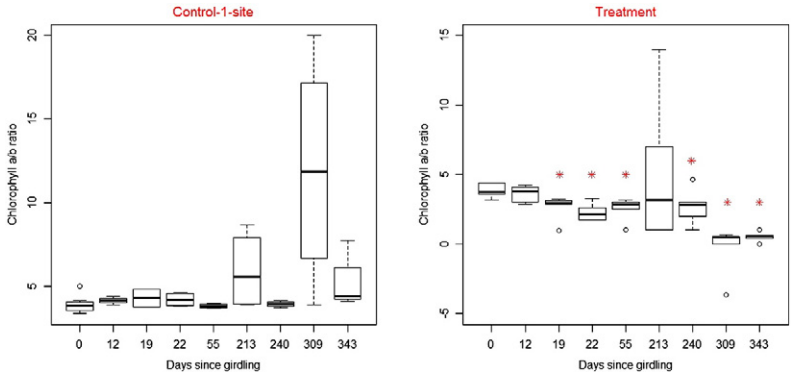


**Fig. 2.** Chlorophyll a/b ratio measured at the control-1-site and the treatment site. A statistically significant decrease in the chlorophyll a/b ratio compared to the chlorophyll a/b ratio before the girdling is marked by an asterisk.

to be superior to red and green band information in terms of its responsiveness to stress induced changes in $Chl_{ab}$ (Carter, 1993, 1998; Carter & Knapp, 2001; Carter & Miller, 1994; Eitel et al., 2007, 2008, 2009, 2010). To our knowledge, this study is the first to confirm that broadband satellite data containing the red-edge band is useful and important as a sensitive indicator for monitoring forest health at the landscape scale.

The NDVI was insensitive to early stress 25 days after girdling likely because $Chl_{ab}$ values remained $>30\ \mu g\ cm^{-2}$ throughout this period. In contrast, the NDVI dropped in value when $Chl_{ab}$ fell below $30\ \mu g\ cm^{-2}$ shortly after 25 days after gridling. As shown by the PROSPECT + SAIL simulated results (Fig. 1), NDVI is not responsive to $Chl_{ab}$ changes $>30\ \mu g\ cm^{-2}$, but becomes responsive to $Chl_{ab}$ changes $<30\ \mu g\ cm^{-2}$. Unexpectedly, we found that GNDVI did not detect $Chl_{ab}$-related stress earlier than NDVI. Further, while GNDVI values dropped below the "no change" zone on day 29 post-girdling, it returned to the "no change" zone between 54 and 74 days post-girdling before again permanently dropping below the "no change" zone. The exact reason for this behavior is unknown yet may represent sensitivity to confounding factors such as atmospheric or BRDF effects that introduced some noise that could not be accounted for in the detrending. While further research may be warranted to explore the exact reasons for this behavior, we note that a similar rebound occurred in both the NDVI and NDRE time series, however, the latter indices had dipped farther below the "no change" region.

In this study, a trained interpreter selected the pixels of girdled and non-girdled trees, which might have affected the results. Therefore, a repeat analysis was conducted after selecting a second independent set of treatment and control pixels, which yielded comparable results.

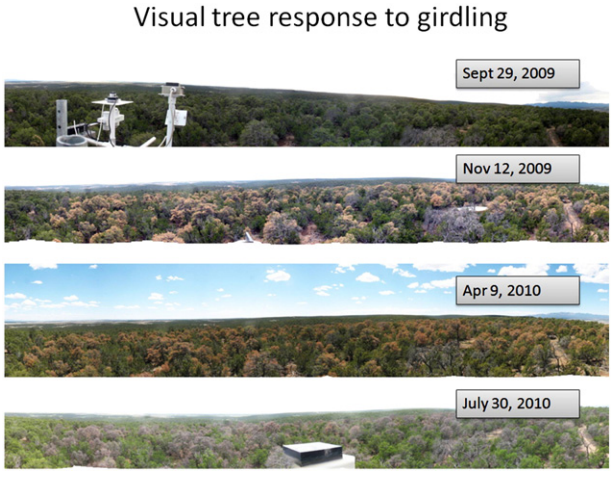


**Fig. 3.** Visual changes in tree greenness taken at intervals throughout the experiment.

In addition, defining the no change region by the 25th and 75th percentile of SVI values measured during no stress conditions is somewhat arbitrary and may need to be adjusted for different locations or agents of stress. Nevertheless, NDRE was most responsive to early stages of $Chl_{ab}$-signified stress as indicated by a pronounced drop in the average SI values 13 days after girdling; a time occurring between 12 and 16 days before NDVI and GNDVI showed a pronounced drop.

The suitability of wavebands and associated spectral indices for stress detection varied throughout the progression of the stress-induced disturbance. The NDVI was less suitable for early stress detection than NDRE. However, during later stress stages (54 to 377 days since girdling) characterized by very low chlorophyll a/b ratios and eventually changes in leaf area, NDVI remained responsive to those changes whereas NDRE remained unchanged. This finding is in broad agreement with findings by Hilker et al. (2009) who showed that the wavebands suitable for detection of mountain pine beetle induced disturbance varied with stage of disturbance. This finding is further supported by the PROSPECT + SAIL model simulation results in Fig. 1 showing a steeper slope and thus sensitivity of NDVI to low $Chl_{ab}$ ($<20\ \mu g\ cm^{-2}$) versus that of GNDVI and NDRE.

In this study, all indices employed spectral bands that are mainly sensitive to stress induced variations in $Chl_{ab}$ (visible bands) and biomass (NIR band). Another important indicator of forest health is plant water status, which is also important in semi-arid piñon-juniper woodlands and other water limiting ecosystems (Stimson et al., 2005). Chronic decreases in foliar water content decreases plant transpiration and carbon gain, which can lead to higher susceptibility to other plant stresses and result in mortality (Breshears et al., 2009). Water stressed plants can also be more susceptible to insects and diseases (Breshears et al., 2009). This suggests that a satellite based early warning system in water-limited ecosystems should ideally rely on both — remote sensing matrices that are sensitive to variations in plant water status and $Chl_{ab}$ (e.g., NDRE as has been shown in this study).

Based on our results, the application of a satellite platform that provides red-edge band information appears promising for the development of a wildland early warning system for land management organizations. Earth observation platforms have been widely applied to forest disturbance and health problems, and examples exist for mapping vegetation change, fire occurrence, fuel, post-fire severity, insects and disease defoliation, plant stress, and biodiversity (e.g. Meddens et al., 2011; Suárez et al., 2009). The focus of much of this work is the rapid and low cost detection of chronic and episodic forest disturbance as part of large scale monitoring by land management agencies (Bennett & Tkacz, 2008). Proposed early warning systems for wildlands in the United States rely on NDVI values derived from the Moderate Resolution Imaging Spectroradiometer (MODIS) (Hargrove et al., 2009). In this system, deviations between current and historical MODIS data (Liang & Schwartz, 2009) are mapped at weekly intervals to detect

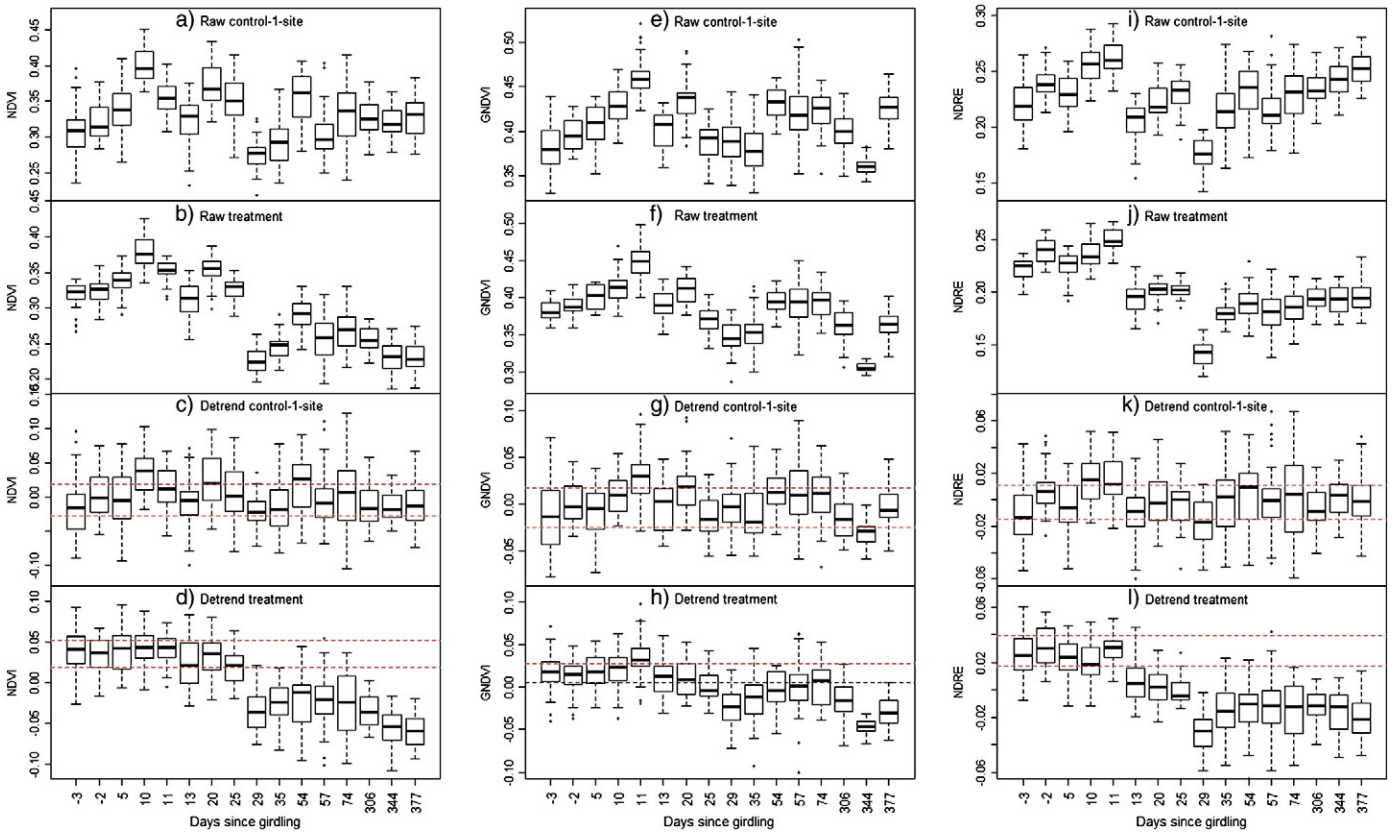


**Fig. 4.** Raw and detrended spectral indices observed in the control-1-site (n = 40) and treatment site (n = 40). Upper and lower dotted red lines encompass the "no change" region. The no change region was defined by the 25th and the 75th percentile of spectral index values measured before the girdling (07-Sept-09; 08-Sept-09). An area was classified as stressed if the 75th percentile of SVI values within the studied area dropped below the no change region.

locations of major phenological change for the conterminous United States. Deviations from "normal" land surface phenological development have been documented as early indicators of changes in forest conditions (de Beurs & Henebry, 2005; Hargrove et al., 2009; Liang & Schwartz, 2009; Morisette et al., 2009). The current study showed that the satellite platforms that provide red-edge band information may well be capable of detecting stress earlier than those without red-edge band information.

One problem where our method may hold promise is the monitoring of mountain pine beetle attacks (Raffa et al., 2008; Wulder et al., 2009). While detection of the mountain pine beetle red attack stage is relatively straightforward (e.g., Wulder et al., 2009), the detection of green attack trees for use in an early warning system has not been demonstrated. Based on the results of the current study, satellite platforms that provide red-edge band information are potentially useful for detecting bark beetle attacks during the green attack stage. Mapping green attack trees relating to ongoing bark beetle epidemics would allow for increased efficiency of beetle treatment and control. Further research is needed to test if satellite platforms that provide red-edge band information allow effective detection of bark beetle attacks during the green attack stage.

## 4. Conclusion

A broadband SVI incorporating the red-edge $Chl_{ab}$ detection band detected plant foliar stress as related to $Chl_{ab}$ changes earlier than other broadband SVIs incorporating the green and red $Chl_{ab}$ detection bands. This finding is mainly explained by the sensitivity of the red-edge band to stress induced changes in $Chl_{ab}$ and possibly due to the sensitivity of the red-edge band to stressed induced increase in fluorescence. However, during later stages of stress, characterized by low $Chl_{ab}$ levels ($<30\ \mu g\ cm^{-2}$) and needle loss, NDVI shows to be more indicative to stress related changes than NDRE.

## Acknowledgments

We greatly appreciate John McCallum for processing and analyzing leaf samples in the laboratory. We also thank RapidEye for making the dense timeseries of imagery available for this study. This work was supported by a cooperative agreement between the University of Idaho and USDA, Forest Service Pacific Northwest Research Station agreement 10JV11261900065, and by the University of Idaho Harold Heady Professorship. We thank two anonymous reviewers for their helpful comments on earlier versions of the manuscript.

## References

Alonso, M., Rozados, M. J., Vega, J. A., Pérez-Gorostiaga, P., Cuiñas, P., Fontúrbel, M. T., & Fernández, C. (2002). Biochemical responses of *Pinus pinaster* trees to fire-induced trunk girdling and crown scorch: secondary metabolites and pigments as needle chemical indicators. *Journal of Chemical Ecology*, *28*, 687–700.

Barnes, E. M., Clarke, T. R., Richards, S. E., Colaizzi, P. D., Haberland, J., Kostrzewski, M., Waller, P., Choi, C., Riley, E., Thompson, T., Lascano, R. J., Li, H., & Moran, M. S. (2000). *Coincident detection of crop water stress, nitrogen status and canopy density using ground-based multispectral data [CD Rom]*. Proceedings of the Fifth International Conference on Precision Agriculture, Bloomington, MN, USA, 16–19 July 2000.

Bennett, D. D., & Tkacz, B. M. (2008). Forest health monitoring in the United States: a program overview. *Australian Forestry*, *71*, 223–228.

Breshears, D. D., Myers, O. B., Meyer, C. W., Barnes, F. J., Zou, C. B., Allen, C. D., McDowell, N. G., & Pockman, W. T. (2009). Tree die-off in response to global change-type drought: mortality insights from a decade of plant water potential measurements. *Frontiers in Ecology and the Environment*, *7*, 185–189.

Carter, G., Cibula, W., & Miller, R. L. (1996). Narrow-band reflectance imagery compared with thermal imagery for early detection of plant stress. *Journal of Plant Physiology*, *148*, 515–522.

Carter, G. A. (1993). Response of leaf spectral reflectance to plant stress. *American Journal of Botany*, *80*, 239–243.
Carter, G. A. (1998). Reflectance wavebands and indices for remote estimation of photosynthesis and stomatal conductance in pine canopies. *Remote Sensing of Environment*, *63*, 61–72.
Carter, G. A., & Knapp, A. K. (2001). Leaf optical properties in higher plants: linking spectral characteristics to stress and chlorophyll concentration. *American Journal of Botany*, *88*, 677–684.
Carter, G. A., & Miller, R. L. (1994). Early detection of plant stress by digital imaging within narrow stress-sensitive wavebands. *Remote Sensing of Environment*, *50*, 295–302.
Ceccato, P., Flasse, S., Tarantola, S., Jacquemoud, S., & Gregoir, J. M. (2001). Detecting vegetation leaf water content using reflectance in the optical domain. *Remote Sensing of Environment*, *77*, 22–33.
de Beurs, K. M., & Henebry, G. M. (2005). Land surface phenology and temperature variation in the IGBP high-latitude transects. *Global Change Biology*, *11*, 779–790.
Eitel, J. U. H., Gessler, P. E., Smith, A. M. S., & Robberecht, R. (2006). Suitability of existing and novel spectral indices to remotely detect water stress in *Populus* spp. *Forest Ecology and Management*, *229*, 170–182.
Eitel, J. U. H., Keefe, R. F., Long, D. S., Davis, A. S., & Vierling, L. A. (2010). Active ground optical remote sensing for improved monitoring of seedling stress in nurseries. *Sensors*, *10*, 2843–2850.
Eitel, J. U. H., Long, D. S., Gessler, P. E., & Hunt, E. R. (2008). Combined spectral index to improve ground-based estimates of nitrogen status in dryland wheat. *Agronomy Journal*, *100*, 1694–1702.
Eitel, J. U. H., Long, D. S., Gessler, P. E., Hunt, E. R., & Brown, D. J. (2009). Sensitivity of ground-based remote sensing estimates of wheat chlorophyll content to variation in soil reflectance. *Soil Science Society of America Journal*, *73*, 1715–1723.
Eitel, J. U. H., Long, D. S., Gessler, P. E., & Smith, A. M. S. (2007). Using in-situ measurements to evaluate the new RapidEye satellite series for prediction of wheat nitrogen status. *International Journal of Remote Sensing*, *28*, 4183–4190.
Eitel, J. U. H., Vierling, L. A., Long, D. S., Litvak, M., & Eitel, K. C. B. (2011). Simple assessment of needleleaf and broadleaf chlorophyll content using a flatbed color scanner. *Canadian Journal of Forest Research*, *41*, 1445–1451.
Gitelson, A., Merzlyak, M., & Lichtenthaler, H. (1996). Detection of red edge position and chlorophyll content by reflectance measurements near 700 nm. *Journal of Plant Physiology*, *148*, 501–508.
Hargrove, W. W., Spruce, J. P., Gasser, G. E., & Hoffman, F. M. P. E. R. S.-. (2009). Toward a national early warning system for forest disturbances using remotely sensed canopy phenology. *Photogrammetric Engineering and Remote Sensing*, *75*, 1150–1156.
Hatala, J. A., Crabtress, R. L., Halligan, K. Q., & Moorcroft, P. R. (2010). Landscape-scale patterns of forest pest and pathogen damage in the Greater Yellowstone Ecosystem. *Remote Sensing of Environment*, *114*, 375–384.
Hendry, G. A. F., Houghton, J. D., & Brown, S. B. (1987). The degradation of chlorophyll — a biological enigma. *New Phytologist*, *107*, 255–302.
Hilker, T., Coops, N., Coggins, S. B., Wulder, M. A., Brown, M., Black, T. A., Nesic, Z., & Lessard, D. (2009). Detection of foliage conditions and disturbance from multi-angular high spectral resolution remote sensing. *Remote Sensing of Environment*, *113*, 421–434.
Jacquemoud, S., & Baret, F. (1990). PROSPECT: a model of leaf optical properties spectra. *Remote Sensing of Environment*, *34*, 75–91.
Liang, L., & Schwartz, M. D. (2009). Landscape phenology: an integrative approach to seasonal vegetation dynamics. *Landscape Ecology*, *24*, 465–472.
Lichtenthaler, H. K., & Rinderle, U. (1988). The role of chlorophyll fluorescence in the detection of stress conditions in plants. *CRC Critical Reviews in Analytical Chemistry*, *19*, 29–85.
Lichtenthaler, H. K., & Wellburn, A. R. (1983). Determination of total carotenoids and chlorophylls a and b of leaf extracts in different solvents. *Biochemical Society Transactions*, *11*, 591–592.
Logan, J. A., Régnière, J., & Powell, J. A. (2003). Assessing the impacts of global warming on forest pest dynamics. *Frontiers in Ecology and the Environment*, *1*, 130–137.
Luther, J. E., & Carroll, A. L. (1999). Development of an index of balsam fir vigor by foliar spectral reflectance. *Remote Sensing of Environment*, *69*, 241–252.
MacKinney, G. (1941). Absorption of light by chlorophyll solutions. *Journal of Biological Chemistry*, *140*, 315–322.
Meddens, A., Hicke, J. A., & Vierling, L. A. (2011). Evaluating the potential of multispectral imagery for mapping multiple stages of tree mortality. *Remote Sensing of Environment*, *115*, 1632–1642.
Morisette, J. T., Richardson, A. D., Knapp, A. K., Fisher, J. I., Graham, E., Abatzoglou, J., Wilson, B. E., Breshears, D. D., Henebry, G. M., Hanes, J. M., & Liang, L. (2009). Unlocking the rhythm of the seasons in the face of global change: challenges and opportunities for phenological research in the 21st century. *Frontiers in Ecology and the Environment*, *7*, 253–260.
Niinemets, Ü. (2010). Responses of forest trees to single and multiple environmental stresses from seedlings to mature plants: past stress history, stress interactions, tolerance and acclimation. *Forest Ecology and Management*, *260*, 1623–1639.
Ollinger, S. V. (2011). Sources of variability in canopy reflectance and the convergent properties of plants. *New Phytologist*, *189*, 375–394.
Pontius, J., Hallett, R., & Martin, M. (2005). Using AVIRIS to assess hemlock abundance and early decline in the Catskills, New York. *Remote Sensing of Environment*, *97*, 163–173.
R Development Core Team (2010). *R: a language and environment for statistical computing.* Vienna, Austria: R Foundation for Statistical Computing3-900051-07-0, URL http://www.R-project.org/
Raffa, K. F., Aukema, B. H., Bentz, B. J., Carroll, A. L., Hicke, J. A., Turner, M. G., & Romme, W. H. (2008). Cross-scale drivers of natural disturbances prone to anthropogenic amplification: the dynamics of Bark Beetle eruptions. *BioScience*, *58*, 501–517.
RapidEye AG (2011). Satellite imagery product specifications. Version 2.1. May 2011. Source: http://www.rapideye.de/products/ortho.htm. Verified on August 24, 2011.
Stimson, H. C., Breshears, D. D., Ustin, S. L., & Kefauver, S. C. (2005). Spectral sensing of foliar water conditions in two co-occurring conifer species: *Pinus edulis* and *Juniperus monosperma*. *Remote Sensing of Environment*, *96*, 108–118.
Suárez, L., Zarco-Tejada, P. J., Berni, J. A. J., González-Dugo, V., & Fereres, E. (2009). Modeling PRI for water stress detection using radiative transfer models. *Remote Sensing of Environment*, *113*, 730–744.
Toomey, M., & Vierling, L. A. (2005). Multispectral remote sensing of landscape level foliar moisture: techniques and applications for forest ecosystem monitoring. *Canadian Journal of Forest Research*, *35*, 1087–1097.
Trigg, S., & Flasse, S. (2000). Characterizing the spectral–temporal response of burned savannah using in situ spectroradiometry and infrared thermometry. *International Journal of Remote Sensing*, *21*, 3161–3168.
Tucker, C. J. (1979). Red and photographic infrared linear combinations for monitoring vegetation. *Remote Sensing of Environment*, *8*, 127–150.
Verhoef, W. (1984). Light scattering by leaf layers with application to canopy reflectance modeling: the SAIL model. *Remote Sensing of Environment*, *16*, 125–141.
Wulder, M. A., Dymond, C. C., White, J. C., Leckie, D. G., & Carroll, A. L. (2005). Surveying mountain pine beetle damage of forests: a review of remote sensing opportunities. *Forest Ecology and Management*, *221*, 27–41.
Wulder, M. A., White, J. C., Carroll, A. L., & Coops, N. C. (2009). Challenges for the operational detection of mountain pine beetle green attack with remote sensing. *The Forestry Chronicle*, *85*, 32–38.